Benchmarking the ideal sample thickness in cryo-EM

Michael W. Martynowycz[a,b], Max T. B. Clabbers[b], Johan Unge[b], Johan Hattne[a,b], and Tamir Gonen[a,b,c,1]

[a]HHMI, University of California, Los Angeles, CA 90095; [b]Department of Biological Chemistry, University of California, Los Angeles, CA 90095; and [c]Department of Physiology, University of California, Los Angeles, CA 90095

Edited by Yifan Cheng, University of California, San Francisco, CA; received May 12, 2021; accepted October 1, 2021

The relationship between sample thickness and quality of data obtained is investigated by microcrystal electron diffraction (MicroED). Several electron microscopy (EM) grids containing proteinase K microcrystals of similar sizes from the same crystallization batch were prepared. Each grid was transferred into a focused ion beam and a scanning electron microscope in which the crystals were then systematically thinned into lamellae between 95- and 1,650-nm thick. MicroED data were collected at either 120-, 200-, or 300-kV accelerating voltages. Lamellae thicknesses were expressed in multiples of the corresponding inelastic mean free path to allow the results from different acceleration voltages to be compared. The quality of the data and subsequently determined structures were assessed using standard crystallographic measures. Structures were reliably determined with similar quality from crystalline lamellae up to twice the inelastic mean free path. Lower resolution diffraction was observed at three times the mean free path for all three accelerating voltages, but the data quality was insufficient to yield structures. Finally, no coherent diffraction was observed from lamellae thicker than four times the calculated inelastic mean free path. This study benchmarks the ideal specimen thickness with implications for all cryo-EM methods.

Cryo-EM | MicroED | FIB milling | electron scattering | mean free path

High-energy electrons interact strongly with matter (1–3), but this strong interaction also implies a higher probability of an electron scattering multiple times and/or losing energy within the specimen (4). The probability of scattering relates to a physical property known as the mean free path (MFP). This is the average distance traveled through a sample by a moving particle before an interaction takes place. The inelastic MFP refers to the typical distance that a high-energy electron travels through a specimen before losing energy in an inelastic-scattering interaction. This lost energy is deposited into the sample and is responsible for e.g. the decay in sample resolution over time, or radiation damage (5). Following energy loss, inelastically scattered electrons lose coherence, which in turn diminishes the measurable coherent diffraction (6, 7). The MFP increases with acceleration voltage and may be roughly calculated for a given sample in cryo–electron microscopy (cryo-EM), in which it is often used to compare samples of different thicknesses across different accelerating voltages. The MFP has been investigated experimentally in vitreous ice, since this is the most-probable environment in these experiments, though similar values have recently been demonstrated in liquid water (6–9).

Early cryo-EM investigations of electron diffraction from frozen-hydrated protein samples reported measurable differences between the intensities of Friedel mates from two-dimensional crystals of bacteriorhodopsin (bR) (10). These differences were suggested to arise from dynamically scattered electrons, or electrons that interact elastically multiple times on their path through the sample while remaining coherent. Dynamically scattered electrons can introduce significant errors, breaking the relationship between the recorded intensity and the underlying structure factor amplitude. Computational simulations further suggested that dynamical scattering leads to highly inaccurate intensities for two-dimensional crystals of bR thicker than 20 nm at 100 kV and three-dimensional crystals of lysozyme thicker than 100 nm at 200 kV (11, 12). Those simulated results are at odds with experimental reports that diffraction intensities from three-dimensional catalase crystals at 200 kV at which the measured intensities were accurate for thicknesses up to at least 150 nm (13). Indeed, subsequent investigations reported structures of catalase from crystals of variable thicknesses without the need of any dynamical corrections (14, 15). Many macromolecular structures have since been reported from crystals that are significantly thicker than 100 nm using microcrystal electron diffraction (MicroED) (15–21).

Until recently, a systematic investigation of how sample thickness effects data quality was not feasible. This is because there was no good way to control sample thickness of biological material. Now, focused ion beam (FIB) milling allows the thickness of a vitrified sample to be precisely controlled (22–29). This process was originally developed for milling cells and tissue specimens to prepare them for subsequent cryo-tomography investigations (28, 30) and has recently been adapted to milling protein crystals for subsequent MicroED investigations (22–27). For example, Zhou et al. milled several crystals to different thicknesses and compared single diffraction pattern from each at 200 kV (25), but they did not systematically correlate the effect of crystal thickness to the ability to determine structures. Here, we systematically investigated the impact of sample thickness on the quality of attainable data and the ability to determine structures.

Microcrystals of proteinase K were milled into lamellae between 95 and 1,650 nm thick. MicroED data were collected from each lamella at one of the three most-common acceleration voltages (120, 200, and 300 kV) (Fig. 1). Thicknesses were expressed in terms of the inelastic MFP, such that measurements at different accelerating voltages could be compared. These

Significance

A systematic investigation of the effects of sample thickness on electron scattering in electron cryo-microscopy (cryo-EM) was previously not feasible. Here, methods are employed to investigate the effects of increasing sample thickness. Near identical protein crystals are used as samples, and microcrystal electron diffraction data are used to assess the effects of thickness. These experiments were conducted using the three most-common accelerating voltages in cryo-EM, and data were compared using the calculated inelastic mean free path. Structures may be determined using crystals up to twice the inelastic mean free path. No coherent information remains at thicknesses over four times the mean free path. This study provides limits for biological specimen thickness with implications for all cryo-EM methods.

Author contributions: M.W.M. and T.G. designed research; M.W.M., M.T.B.C., and T.G. performed research; M.W.M., M.T.B.C., J.U., J.H., and T.G. analyzed data; and M.W.M., M.T.B.C., J.H., and T.G. wrote the paper.

The authors declare no competing interest.

This article is a PNAS Direct Submission.

[1]To whom correspondence may be addressed. Email: tgonen@g.ucla.edu.

This article contains supporting information online at http://www.pnas.org/lookup/suppl/doi:10.1073/pnas.2108884118/-/DCSupplemental.

Published December 3, 2021.

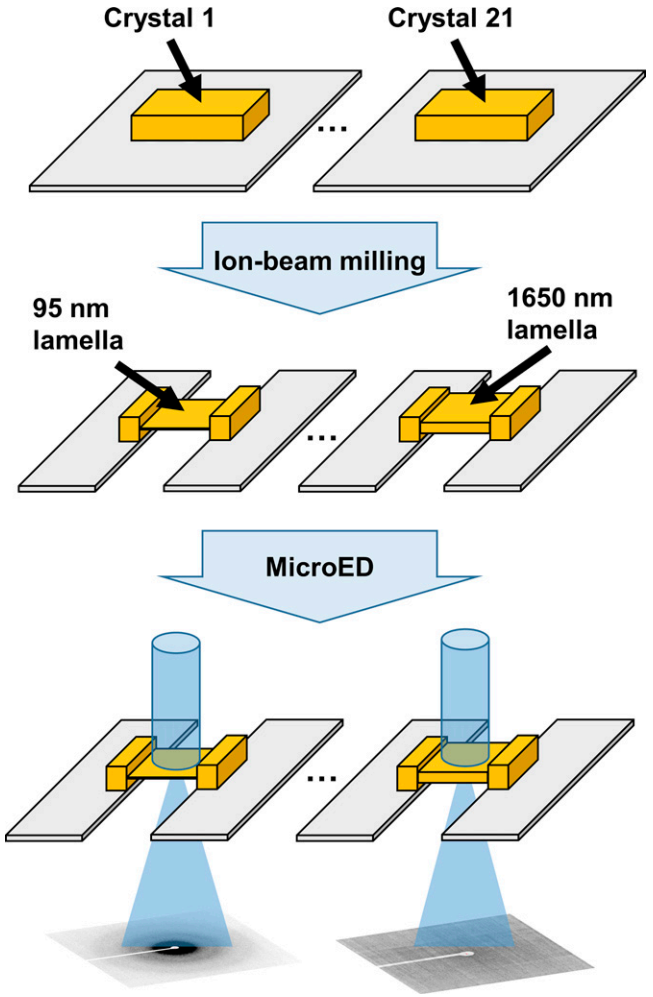

Fig. 1. Preparation of protein microcrystals into lamellae of specified thicknesses. Schematic cartoon showing the general process of systematically investigating data quality for variably thick samples. Crystals are identified on EM grids (*Top*), milled to specified thicknesses (*Middle*), and MicroED datasets are collected from each crystal at either 120-, 200-, or 300-kV accelerating voltages.

thicknesses roughly correspond to between 0.5× and 5×MFP. We found that MicroED data from crystals as thick as twice the MFP provided sufficiently accurate intensities to determine high-resolution protein structures irrespective of the acceleration voltage. Surprisingly, no large difference in data or structure quality was observed from lamellae thinner than 2×MFP. Diffraction was still observed at up to 3×MFP, but the data were not suitable for processing. No diffraction spots were observed for thicknesses beyond 4×MFP. This study provides initial measurements of crystals of definitive thicknesses at varying accelerating voltages and provides a benchmark for limits on biological specimen thickness with implications for all cryo-EM investigations.

Results

Preparing Grids with Protein Crystals. Proteinase K crystals were grown in batch as described (31, 32). This condition results in protein microcrystals that measure between 10 and 30 μm across their middle. Transmission electron microscopy (TEM) grids were prepared by back blotting as described (32). The samples were then loaded into a FIB scanning electron microscope (SEM).

Vitrified grids were coated with sputtered platinum to protect the crystals from the damaging electron and ion beams during investigation (31) (*Materials and Methods*). Each grid was searched using the scanning electron beam for crystals that satisfied the following requirements: each crystal was of relatively similar size, was at least 5 μm away from the nearest grid bar, and at least 3 grid squares away from the edge of the grid. In this way, five appropriate crystals were identified on a first batch of grids, nine on the second, and seven on the third. Each crystal was inspected in both the SEM and FIB and then brought to the eucentric position. Lamellae were milled by rastering the gallium beam across the microcrystals (*Materials and Methods*). The ion beam current was lowered as the desired thickness was approached (28, 31). The thickness of each crystalline lamella was measured by taking an image in the ion beam just prior to unloading each grid. These measurements are accurate to ∼5 to 10 nm for the individual crystalline lamellae but can underestimate the final thickness due to the accumulation of amorphous ice or contaminants during storage and transfer of the grids (*Materials and Methods*). We are therefore reporting the minimum thickness for each lamella. Lamellae thicknesses spanned from ∼95 to 1,650 nm (Figs. 1 and 2) (*Materials and Methods*).

MicroED Experiments on Crystalline Lamellae. Each grid was carefully rotated by 90° when loading into the TEM, such that the rotation axis in the TEM was perpendicular to the milling direction in the FIB/SEM. This means that the lamellae were not perpendicular to the electron beam at zero stage tilt but offset by 18°. Samples were investigated at an accelerating voltage of either 120, 200, or 300 kV. Lamellae on each grid were identified by low-magnification montaging, and the eucentric height was adjusted individually for each site. A selected area aperture was used to isolate the diffraction from a circular area ∼3 μm in

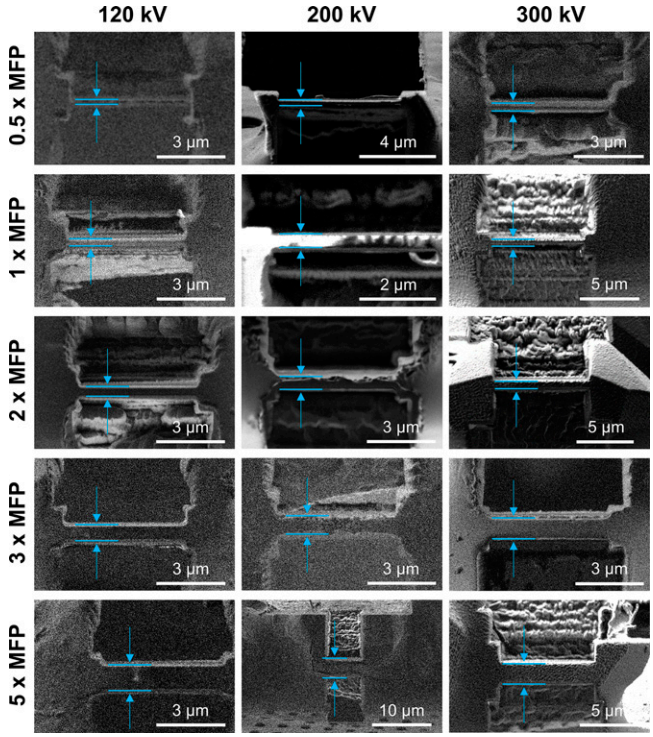

Fig. 2. Preparing protein lamellae of variable thicknesses. Images taken by the gallium ion beam of selected crystalline lamellae after milling. Images are sorted into rows and columns by the accelerating voltages used for data collection and the calculated multiple of the inelastic MFP for protein for that condition. Approximate location and size of lamellae are indicated by blue arrows and blue lines.

diameter from the center of each lamella. In this way, no diffraction or signal from anything other than the thickness-controlled lamellae was recorded during data collection. Continuous rotation MicroED data were collected from each lamella while continuously rotating the stage from 30° to −30° (Fig. 3).

Data from each lamella were converted to crystallographic format (Fig. 3 and *SI Appendix*, Figs. 1–36). An initial, subjective estimate of the scattering resolution from each lamella was obtained by visually inspecting the maximum projection of the corresponding dataset (*Materials and Methods*). The datasets were then indexed, integrated, and scaled individually as described (33). A resolution cutoff was applied to each dataset in which the $CC_{1/2}$ value fell to ∼33% (Table 1) (34). Collectively, strong and sharp reflections were observed from crystal lamellae that were up to 2×MFP thick at the three acceleration voltages. Little or poor diffraction was observed at 3×MFP, while no diffraction could be observed beyond 4×MFP (Fig. 3). Lamellae that yielded usable data were individually integrated and their respective models refined (Table 1 and *SI Appendix*, Table 1). In all cases, the calculated maps and composite omit maps were of high quality (Fig. 4 and *SI Appendix*, Fig. 37).

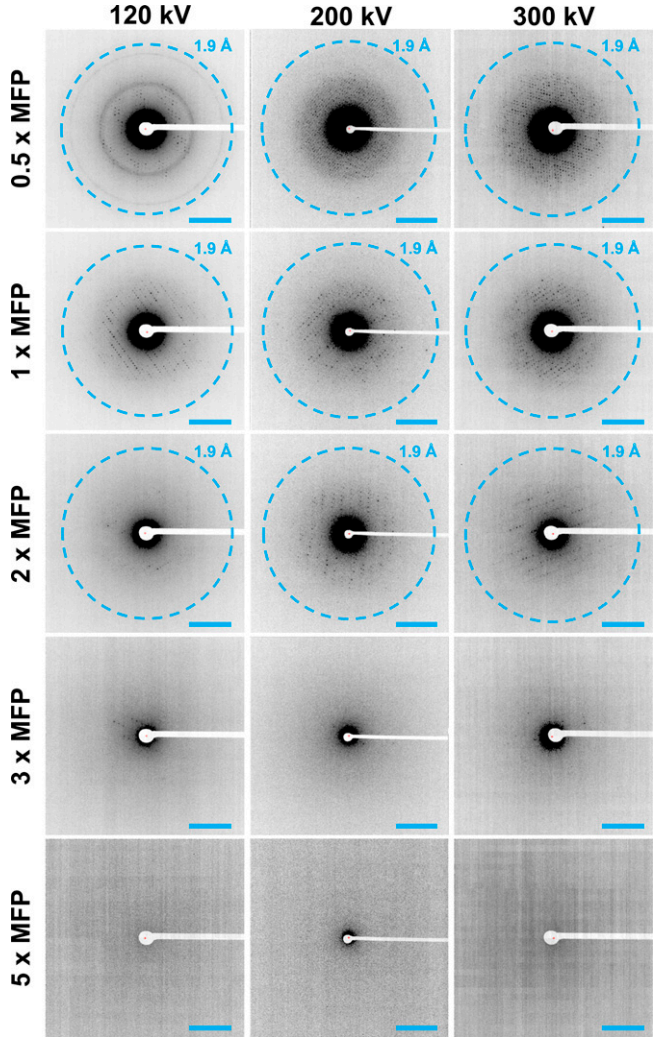

Fig. 3. MicroED data from lamellae of different thicknesses and accelerating voltages. Single frames from MicroED datasets corresponding to 0° stage tilt. Frames are sorted into columns by the accelerating voltage and rows for the approximate thickness expressed as a multiple of the calculated inelastic MFP at that accelerating voltage. (Scale bars, 0.25 $Å^{-1}$.)

Discussion

The relationship between crystal thickness, acceleration voltage, the quality of MicroED data, and the subsequently determined structures was systematically investigated. The samples used were of the same protein, grown in the same batch from crystals of originally similar size, and machined into lamellae using the same protocol (*Materials and Methods*). MicroED data were collected using established procedures (18, 24, 35) at the three most-common acceleration voltages used in cryo-EM: 120, 200, and 300 kV. No systematic errors prevented structure determination from crystals up to twice the MFP. Indeed, the crystallographic statistics, metrics of the determined structures, and resulting maps from lamellae up to 2×MFP all appear relatively similar (Table 1 and Fig. 5). It has been suggested that thinner lamellae should yield better data, and there is some evidence of this in our measurements (Fig. 5 and Table 1), but thin lamellae are also more likely to bend and deform (25). These effects as well as the reduced scattering power from thinner samples with fewer unit cells diffracting in the beam may offset the signal-to-noise benefits of thinner lamellae. Beyond 2×MFP, the overall resolution and quality metrics rapidly fall off (Fig. 5). No structures could be determined at 3×MFP for all acceleration voltages, although sporadic diffraction spots at low resolution were visible on some images. No diffraction was observed for samples thicker than 4×MFP, suggesting that most of the electrons have scattered inelastically within the sample. These observations are in agreement with the measurements of single diffraction patterns from Zhou et al. (25), in which the best data were observed at intermediate thicknesses rather than at an extremum.

The data suggests that the largest detriment to determining structures by MicroED from thicker samples appears to be inelastic scattering within the sample. Since inelastic interactions become more probable as the energy of an electron decreases, the rate at which electrons deposit energy to the sample rapidly increases. Electrons need not deposit all their energy to the sample to reduce the signal in the recorded diffraction pattern, since even partial energy loss will reduce the coherence of the scattered beam. For the purpose of this study, we do not differentiate between partial and total energy loss. These effects are further compounded by the fact that thicker crystals produce more diffuse scattering, and increased inelastic scattering results in higher background noise. Taken together, it is clear that the elastic Bragg peaks are diminished in thick samples and that the higher-resolution reflections are lost to additional noise from the increased background. It is possible that an energy filter could help mitigate some of these issues, and we expect that the usable thickness could slightly increase with the addition of an energy filter. Initial results already demonstrated that an energy filter leads to an increase in the signal-to-noise ratio and the attainable resolution (36–39).

Computer simulations are at odds with results from MicroED experiments. All simulations are inherently limited by the validity of their assumptions, as discussed in Subramanian et al. (11). We suggest that at least five assumptions are inadequate in most electron diffraction simulations: 1) macromolecular crystals are perfect, 2) diffraction is collected with the beam parallel to a major zone axis, which is always true for two-dimensional (2D) crystals but rarely for three-dimensional (3D) crystals, 3) contribution from disordered solvent is negligible, 4) data are collected from stationary crystals (MicroED uses continuous rotation), and 5) inelastic scattering or absorption is insignificant. Though more recent simulations have made progress in accounting for some of these discrepancies (40), future simulations may benefit from a more accurate modeling of the experimental setup.

Results from simulations, 2D crystals, and materials science would suggest that dynamical scattering is detrimental for EM studies of samples even just 100 nm thick (11). Dynamical-

Table 1. MicroED data from crystal lamellae of specified thicknesses

Crystal #	1	2	3	4	5	6	7	8	9
120 kV									
Thickness (nm)	130	200	325	600	960				
MFP (×)	0.6	0.9	1.5	2.8	4.5				
Resolution limit (Å)	2.3	2.0	2.7	3.8*	20**				
Completeness (%)	82.5	87.7	82.6	—	—				
R_{pim} (%)	14.9	12.8	29.6	—	—				
$\langle I/\sigma(I)\rangle$	5.0	4.9	3.2	0***	0***				
$CC_{1/2}$	97.5	98.3	89.3	0***	0***				
R_{work} (%)	22.2	21.5	24.1	—	—				
R_{free} (%)	26.1	24.3	28.5	—	—				
200 kV									
Thickness (nm)	95	115	130	260	460	530	540	800	1400
MFP (×)	0.3	0.4	0.5	1	1.7	1.95	2	2.9	5.1
Resolution limit (Å)	2.35	1.85	1.95	1.95	1.95	2.3	2.4	4.1*	20**
Completeness (%)	86.6	86.0	96.8	91.1	91.9	90.0	78.6	—	—
R_{pim} (%)	15.9	10.8	13.4	13.3	15.4	19.7	15.6	—	—
$\langle I/\sigma(I)\rangle$	3.6	5.2	4.4	4.25	3.85	4.41	3.25	—	—
$CC_{1/2}$ (%)	96.8	98.8	97.9	97.6	96.3	91.7	92.5	0***	0***
R_{work} (%)	20.0	18.1	19.4	18.7	20.1	20.1	19.3	—	—
R_{free} (%)	24.0	21.7	23.6	23.9	24.5	24.1	22.2	—	—
300 kV									
Thickness (nm)	150	170	320	360	550	880	1650		
MFP (×)	0.47	0.54	1.0	1.2	1.7	2.8	5.2		
Resolution limit (Å)	1.9	2.1	2.1	2.05	2.9	3.7*	20**		
Completeness (%)	90.5	89.9	82.5	92.9	90	—	—		
R_{pim} (%)	11.8	32.4	14.4	12.8	23.1	—	—		
$\langle I/\sigma(I)\rangle$	4.9	3.38	3.61	3.8	2.43	—	—		
$CC_{1/2}$ (%)	98.5	91.7	96.4	95.6	77.3	0***	0***		
R_{work} (%)	19.17	27.25	19.85	19.14	23.8	—	—		
R_{free} (%)	22.64	33.20	24.46	23.64	27.45	—	—		

*Value approximated from diffraction images that could not be automatically processed.
**Best possible value given experimental cutoff due to beamstop.
***Value presumed from inability to integrate datasets.

scattering effects in single-particle cryo-EM experiments are of little concern, since the sample thickness is typically much thinner than MicroED or tomography experiments (~10 to 20 nm) (41, 42). Cryogenic electron tomography experiments are typically conducted on frozen cells or tissues that can be microns thick (43). These specimens are often also milled to thin lamellae to increase the achievable resolution and reduce the noise (28, 30). Identifying at what thickness useful information can be obtained is challenging using imaging techniques, since factors such as drift, charging, and other aberrations can be difficult to control and correct. Our results provide experimentally determined benchmarking of ideal sample thicknesses for the common acceleration voltages in cryo-EM of biological material using diffraction, which is a definitive measure of information obtainable at specific resolutions.

We demonstrated that high-quality structures can be obtained from samples that are up to 2× the MFP regardless of the acceleration voltage. This corresponds to physical sample thicknesses of ~430, 540, and 640 nm for the accelerating voltages of 120, 200, and 300 kV, respectively. We find that samples that were thicker did not yield usable data, and thicknesses greater than 4×MFP did not yield any useful diffraction data. We expect that these limits could be somewhat relaxed with an energy filter, but the exact parameters will need to be investigated in future studies. Importantly, as FIB milling becomes a standard method for sample preparation for macromolecular MicroED studies, aiming for thicknesses of less than 2×MFP will maximize the likelihood of producing the best data and highest-quality structures. Regardless of the cryo-EM method employed, the current study provides a benchmark for the sample thickness in cryo-EM.

Materials and Methods

Materials. Proteinase K (*E. Album*) and ammonium sulfate were purchased from Sigma (Sigma-Aldrich, St. Louis) and used without further purification. Stock solutions were made using Milli-Q water filtered three times through a 0.4-μm porous membrane.

Crystallization. Proteinase K was crystallized in batch by dissolving 1 mg of lyophilized protein powder with 200 L of 2 M ammonium sulfate at room temperature. Crystals between 10 and 30 μm formed within 10 min.

Grid Preparation. Quantifoil Cu 200 R 2/2 grids were glow discharged for 30 s immediately prior to use. Grids were vitrified using a Leica GP2 vitrification robot at room temperature. The sample chamber was set to 95% relative humidity and the filter paper equilibrated in the humid air for 15 min prior to grid preparation. The tube of crystals was gently shaken just before 3 L of protein crystal solution was removed and gently pipetted onto the carbon side of the grid in the vitrification chamber. The slurry was incubated on the grid for 30 s. The grid was then gently blotted from the back for 20 s, plunged into liquid ethane, and transferred to liquid nitrogen for storage.

FIB/SEM. Vitrified grids were transferred into a cryogenically cooled Thermo Fisher Scientific Aquilos dual-beam FIB/SEM. The grids were coated in a thin layer of fine platinum followed by a thick >100-nm layer of coarse platinum by sputter coating to protect the crystals from the damaging ion and electron beams (31). Whole-grid atlases were recorded using the MAPS software (Thermo Fisher Scientific), in which individual crystals were identified and aligned to eucentric height. A total 21 crystals over six grids were chosen for milling. Crystals were milled as described (24, 31, 32, 44, 45). Briefly, milling was conducted in steps of rough and fine milling followed by polishing. Each step was performed on each crystal sequentially prior to advancing to the next step to reduce the effects of amorphous ice buildup and contamination. Rough-milling steps were conducted at 100 pA and removed all but 5 μm of crystalline material. Fine milling used an ion beam current of 50 pA and

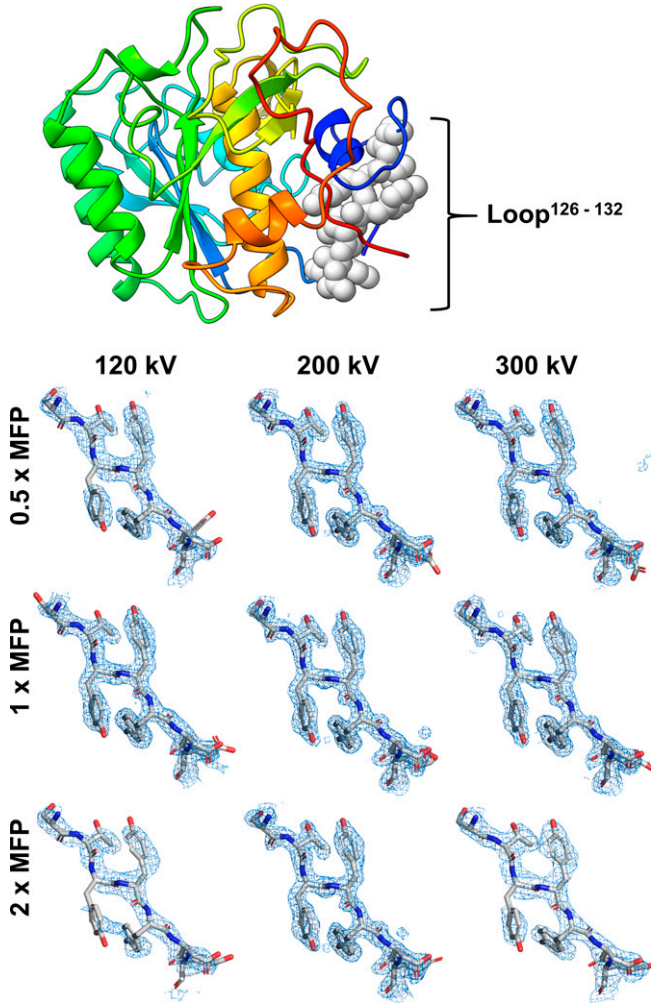

Fig. 4. MicroED structures determined from lamellae of specified thicknesses. (*Top*) Final structure solution of proteinase K in rainbow by residue number with a loop corresponding to residues 126 through 132 shown as gray spheres. (*Bottom*) $2mF_o - F_c$ maps from lamellae of different thicknesses and resolution cutoffs for the selected loop from above. All maps contoured at 1.5 σ with a 2-Å carve.

removed material up to 250 nm away from the desired thickness. Polishing was conducted at an ion beam current of 10 pA and was used until the approximate final thickness was achieved. A final image of the lamella was taken using the ion beam at 1.5 pA (Fig. 2 and *SI Appendix*, Figs. 1–36) to assess the final thickness using the measurement tool in the Aquilos user interface. All micrographs taken by the scanning electron beam were performed at an accelerating voltage of 5 kV and a beam current of 1.6 pA. All ion beam imaging and milling was conducted at an accelerating voltage of 30 kV.

MicroED Data Collection. Grids containing milled lamellae were transferred to either a Thermo Fisher Scientific Titan Krios G3i or Talos Arctica transmission electron microscope. The Krios was operated at an accelerating voltage of either 120 or 300 kV, whereas the Arctica operated at an accelerating voltage of 200 kV. Electrons at the accelerating voltages of 120, 200, or 300 kV have corresponding de Broglie wavelengths of 0.0335 Å, 0.0251 Å, or 0.0197 Å, respectively. Both microscopes were equipped with a field emission gun and a CetaD 16M (4k×4k) camera based on complementary metal-oxide-semiconductor (CMOS) technology. Lamellae were identified on each grid by taking a low-magnification montage, in which they appeared as thin, white stripes against an otherwise dark background. Crystalline lamellae within these strips appeared semitransparent and suspended over this gap. Lamellae were brought to eucentric height and initially evaluated by taking a single 1-s exposure in diffraction mode at 0° stage tilt. MicroED data were collected as described (35). In short, the stage was continuously rotated at a rate of $0.25^\circ\ s^{-1}$ while the crystal was illuminated in a parallel electron beam. Frames were read out from the detector every 1 or 2 s and saved as a stack in MRC format. Each dataset consisted of 120 to 240 images, corresponding to the real-space angular wedge between +30 and −30°. The electron beam was ∼10 μm in diameter, in which the corresponding exposure was calibrated to a rate of $\sim 0.01\ e^-\ Å^{-2}\ s^{-1}$. The total exposure to each lamellae was therefore $\sim 2.4\ e^-\ Å^{-2}$. Signal from the center of each lamella was isolated by inserting a selected area aperture of 100 μm for the Arctica or 150 μm for the Krios, corresponding to an area of ∼3 μm in diameter projected from the sample for either microscope.

MicroED Data Processing. MRC stacks were converted to individual frames in SMV format using the MicroED tools (24, 35). MicroED tools can be downloaded freely at (https://cryoem.ucla.edu/downloads). An offset of 512 analog-to-digital units (ADU) s was added during the conversion of the movies into SMV format to prevent truncation of the negative values read out by the detector (46). Reflections were indexed and integrated in XDS taking the offset into account (33). Individual or groups of datasets were scaled in either AIMLESS (47) or XSCALE (48). Each dataset was phased by molecular replacement in Phaser using Protein Data Bank (PDB) ID 6CL7 (5, 49) as a search model. Models were refined in phenix.refine (50) using electron-scattering factors.

Calculations. The inelastic MFP was calculated using the original formulation by Malis et al. (6) and Egerton et al. (8) and subsequently used by Feja et al. (9) and Grimm et al. (51) given by:

$$\Lambda = \frac{106F\left(\frac{E_0}{E_m}\right)}{\ln\left(\frac{2\rho E_0}{E_m}\right)},$$

and

$$F = \frac{\left(1+\frac{E_0}{1022}\right)}{\left(1+\frac{E_0}{511}\right)^2},$$

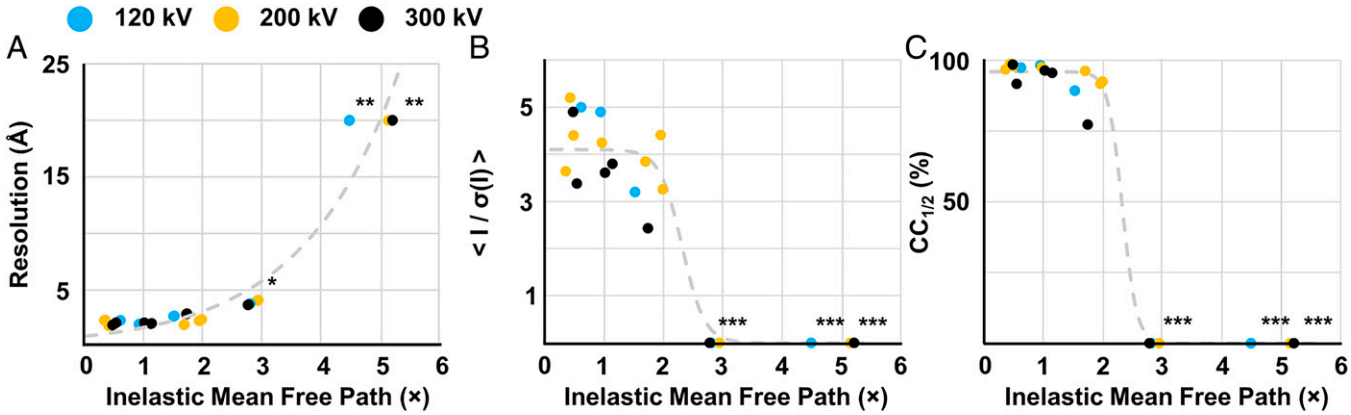

Fig. 5. Data quality metrics as a function of thickness. (*A*) Resolution cutoff, (*B*) mean signal to noise, and (*C*) the half-set correlation coefficient for all the measured crystals. Data points are color coded according to accelerating voltage as indicated. A simple exponential function is fit to the data in *A* and reverse sigmoid functions to the data in *B* and *C* to illustrate the sharp changes after ∼2×MFP. (**) and (***) as defined in Table 1.

where

$$E_m = 7.6\ Z^{0.36}.$$

We similarly used the values of $\beta = 10$ mrad, Z = 8. E_0 is the acceleration voltage (i.e., 120, 200, or 300 kV).

An optical refractive term was applied as suggested by Grimm et al. (51), and a value of $n = 1.48$ was chosen based on the determined value for lysozyme layers (52). This translates to inelastic MFP values of 214, 272, and 317 nm for 120, 200, and 300 kV accelerating voltages. These values are in good agreement with those previously measured experimentally (6–9, 51, 53) and have a direct relationship to the deposited dose (54).

The MFP is closely related to the collision stopping power, as calculated using, for example, ESTAR (55). For a typical protein sample with density 1.17 g cm^{-3} (56), the tabulated stopping power implies that a 120-kV electron loses 4.15 MeV per cm of traversed sample (3.22 MeV and 2.72 MeV for 200 kV and 300 kV electrons, respectively). The deposited energy per unit length calculated by this method was previously used to derive estimates of the dose from a given exposure (5, 54), and its inverse is correlated to the MFP length used here with an asymptotic SE of <2%.

The curves presented in Fig. 5 *B* and *C* are reverse sigmoid functions of the form:

$$f(x) = a^* \frac{1}{1 + e^{b(x-c)}}.$$

The curve presented in Fig. 5*A* is a simple exponential function. Functions were fit using least squares.

Maximum Projection. An estimate of resolution for a complete dataset can be obtained by visually inspecting the projection of maximum intensities through a dataset. The value of each pixel in a maximum projection is highest value of the pixel in all frames that constitute the dataset. The maximum projections calculated by, for example, FIJI (57) provide a way to visually inspect the scattering power from weak datasets, in which the number of strong spots on each individual frame is very low. The projections for all the lamellae (*SI Appendix*, Figs. 1–36) corroborate the general trends seen in the integration statistics (Table 1) and confirm that measurements at 5×MFP are essentially void of diffraction. This suggests that every electron has inelastically scattered at least once, resulting in no coherent diffraction pattern being formed (*SI Appendix*, Figs. 24 and 36).

Data Availability. All study data are included in the article and/or *SI Appendix*. The coordinates and structure factors for the atomic models in this study have been deposited to the PDB under accession codes 7SVY, 7SVZ, 7SW0, 7SW1, 7SW2, 7SW3, 7SW4, 7SW5, 7SW6, 7SW7, 7SW8, 7SW9, 7SWA, 7SWB, and 7SWC. The corresponding density maps have been deposited to the EMDB under codes EMD-25456–EMD-25470.

ACKNOWLEDGMENTS. This study was supported by NIH Grant P41GM136508. The T.G. laboratory is supported by the Howard Hughes Medical Institute.

1. J. M. Cowley, A. F. Moodie, The scattering of electrons by atoms and crystals. I. A new theoretical approach. *Acta Crystallogr.* **10**, 609–619 (1957).
2. R. Henderson, The potential and limitations of neutrons, electrons and X-rays for atomic resolution microscopy of unstained biological molecules. *Q. Rev. Biophys.* **28**, 171–193 (1995).
3. B. K. Vainshtein, E. Feigl, J. A. Spink, *Structure Analysis by Electron Diffraction* (Elsevier Science, 2014).
4. K. Fujiwara, Application of higher order born approximation to multiple elastic scattering of electrons by crystals. *J. Phys. Soc. Jpn.* **14**, 1513–1524 (1959).
5. J. Hattne *et al.*, Analysis of global and site-specific radiation damage in cryo-EM. *Structure* **26**, 759–766.e4 (2018).
6. T. Malis, S. C. Cheng, R. F. Egerton, EELS log-ratio technique for specimen-thickness measurement in the TEM. *J. Electron Microsc. Tech.* **8**, 193–200 (1988).
7. M. N. Yesibolati *et al.*, Electron inelastic mean free path in water. *Nanoscale* **12**, 20649–20657 (2020).
8. R. F. Egerton, S. C. Cheng, Measurement of local thickness by electron energy-loss spectroscopy. *Ultramicroscopy* **21**, 231–244 (1987).
9. B. Feja, U. Aebi, Determination of the inelastic mean free path of electrons in vitrified ice layers for on-line thickness measurements by zero-loss imaging. *J. Microsc.* **193**, 15–19 (1999).
10. R. M. Glaeser, T. A. Ceska, High-voltage electron diffraction from bacteriorhodopsin (purple membrane) is measurably dynamical. *Acta Crystallogr. A* **45**, 620–628 (1989).
11. G. Subramanian, S. Basu, H. Liu, J.-M. Zuo, J. C. H. Spence, Solving protein nanocrystals by cryo-EM diffraction: Multiple scattering artifacts. *Ultramicroscopy* **148**, 87–93 (2015).
12. R. M. Glaeser, K. H. Downing, High-resolution electron crystallography of protein molecules. *Ultramicroscopy* **52**, 478–486 (1993).
13. D. L. Dorset, D. F. Parsons, Electron diffraction from single, fully-hydrated, ox-liver catalase microcrystals. *Acta Crystallogr. A* **31**, 210–215 (1975).
14. B. L. Nannenga, D. Shi, J. Hattne, F. E. Reyes, T. Gonen, Structure of catalase determined by MicroED. *eLife* **3**, e03600 (2014).
15. K. Yonekura, K. Kato, M. Ogasawara, M. Tomita, C. Toyoshima, Electron crystallography of ultrathin 3D protein crystals: Atomic model with charges. *Proc. Natl. Acad. Sci. U.S.A.* **112**, 3368–3373 (2015).
16. B. L. Nannenga, T. Gonen, The cryo-EM method microcrystal electron diffraction (MicroED). *Nat. Methods* **16**, 369–379 (2019).
17. D. Shi, B. L. Nannenga, M. G. Iadanza, T. Gonen, Three-dimensional electron crystallography of protein microcrystals. *eLife* **2**, e01345 (2013).
18. B. L. Nannenga, D. Shi, A. G. W. Leslie, T. Gonen, High-resolution structure determination by continuous-rotation data collection in MicroED. *Nat. Methods* **11**, 927–930 (2014).
19. H. Xu *et al.*, Solving a new R2lox protein structure by microcrystal electron diffraction. *Sci. Adv.* **5**, eaax4621 (2019).
20. M. J. de la Cruz *et al.*, Atomic-resolution structures from fragmented protein crystals with the cryoEM method MicroED. *Nat. Methods* **14**, 399–402 (2017).
21. M. T. B. Clabbers *et al.*, MyD88 TIR domain higher-order assembly interactions revealed by microcrystal electron diffraction and serial femtosecond crystallography. *Nat. Commun.* **12**, 2578 (2021).
22. H. M. E. Duyvesteyn *et al.*, Machining protein microcrystals for structure determination by electron diffraction. *Proc. Natl. Acad. Sci. U.S.A.* **115**, 9569–9573 (2018).
23. E. V. Beale *et al.*, A workflow for protein structure determination from thin crystal lamella by micro-electron diffraction. *Front. Mol. Biosci.* **7**, 179 (2020).
24. M. W. Martynowycz, W. Zhao, J. Hattne, G. J. Jensen, T. Gonen, Collection of continuous rotation MicroED data from ion beam-milled crystals of any size. *Structure* **27**, 545–548.e2 (2019).
25. H. Zhou, Z. Luo, X. Li, Using focus ion beam to prepare crystal lamella for electron diffraction. *J. Struct. Biol.* **205**, 59–64 (2019).
26. X. Li, S. Zhang, J. Zhang, F. Sun, *In situ* protein micro-crystal fabrication by cryo-FIB for electron diffraction. *Biophys. Rep.* **4**, 339–347 (2018).
27. V. Polovinkin *et al.*, Demonstration of electron diffraction from membrane protein crystals grown in a lipidic mesophase after lamella preparation by focused ion beam milling at cryogenic temperatures. *J. Appl. Cryst.* **53**, 1416–1424 (2020).
28. M. Marko, C. Hsieh, R. Schalek, J. Frank, C. Mannella, Focused-ion-beam thinning of frozen-hydrated biological specimens for cryo-electron microscopy. *Nat. Methods* **4**, 215–217 (2007).
29. J. M. Medeiros *et al.*, Robust workflow and instrumentation for cryo-focused ion beam milling of samples for electron cryotomography. *Ultramicroscopy* **190**, 1–11 (2018).
30. F. R. Wagner *et al.*, Preparing samples from whole cells using focused-ion-beam milling for cryo-electron tomography. *Nat. Protoc.* **15**, 2041–2070 (2020).
31. M. W. Martynowycz, W. Zhao, J. Hattne, G. J. Jensen, T. Gonen, Qualitative analyses of polishing and precoating FIB milled crystals for MicroED. *Structure* **27**, 1594–1600.e2 (2019).
32. M. W. Martynowycz, T. Gonen, Ligand incorporation into protein microcrystals for MicroED by on-grid soaking.Structure **29**, 88–95.e2 (2021).
33. W. Kabsch, XDS. *Acta Crystallogr. D Biol. Crystallogr.* **66**, 125–132 (2010).
34. P. A. Karplus, K. Diederichs, Linking crystallographic model and data quality. *Science* **336**, 1030–1033 (2012).
35. J. Hattne *et al.*, MicroED data collection and processing. *Acta Crystallogr. A Found. Adv.* **71**, 353–360 (2015).
36. K. Yonekura, T. Ishikawa, S. Maki-Yonekura, A new cryo-EM system for electron 3D crystallography by eEFD. *J. Struct. Biol.* **206**, 243–253 (2019).
37. K. Yonekura, S. Maki-Yonekura, K. Namba, Quantitative comparison of zero-loss and conventional electron diffraction from two-dimensional and thin three-dimensional protein crystals. *Biophys. J.* **82**, 2784–2797 (2002).
38. T. Gonen *et al.*, Lipid-protein interactions in double-layered two-dimensional AQP0 crystals. *Nature* **438**, 633–638 (2005).
39. M. W. Martynowycz, T. Gonen, "Studying membrane protein structures by MicroED" in *Structure and Function of Membrane Proteins*, I. Schmidt-Krey, J. C. Gumbart, Eds. (*Methods in Molecular Biology*, Springer US, 2021), pp. 137–151.
40. T. Latychevskaia, J. P. Abrahams, Inelastic scattering and solvent scattering reduce dynamical diffraction in biological crystals. *Acta Crystallogr. B Struct. Sci. Cryst. Eng. Mater.* **75**, 523–531 (2019).
41. B. Carragher *et al.*, Current outcomes when optimizing 'standard' sample preparation for single-particle cryo-EM. *J. Microsc.* **276**, 39–45 (2019).
42. L. A. Passmore, C. J. Russo, Specimen preparation for high-resolution cryo-EM. *Methods Enzymol.* **579**, 51–86 (2016).
43. D. N. Mastronarde, Automated electron microscope tomography using robust prediction of specimen movements. *J. Struct. Biol.* **152**, 36–51 (2005).
44. M. W. Martynowycz, F. Khan, J. Hattne, J. Abramson, T. Gonen, MicroED structure of lipid-embedded mammalian mitochondrial voltage-dependent anion channel. *Proc. Natl. Acad. Sci. U.S.A.* **117**, 32380–32385 (2020).
45. M. W. Martynowycz *et al.*, MicroED structure of the human adenosine receptor determined from a single nanocrystal in LCP. Proc. Natl. Acad. Sci. U.S.A. **118**, e2106041118 (2021).

46. J. Hattne, D. Shi, M. J. de la Cruz, F. E. Reyes, T. Gonen, Modeling truncated pixel values of faint reflections in MicroED images. *J. Appl. Cryst.* **49**, 1029–1034 (2016).
47. P. R. Evans, G. N. Murshudov, How good are my data and what is the resolution? *Acta Crystallogr. D Biol. Crystallogr.* **69**, 1204–1214 (2013).
48. W. Kabsch, Integration, scaling, space-group assignment and post-refinement. *Acta Crystallogr. D Biol. Crystallogr.* **66**, 133–144 (2010).
49. A. J. McCoy *et al.*, *Phaser* crystallographic software. *J. Appl. Cryst.* **40**, 658–674 (2007).
50. P. V. Afonine *et al.*, Towards automated crystallographic structure refinement with phenix.refine. *Acta Crystallogr. D Biol. Crystallogr.* **68**, 352–367 (2012).
51. R. Grimm, D. Typke, M. Bärmann, W. Baumeister, Determination of the inelastic mean free path in ice by examination of tilted vesicles and automated most probable loss imaging. *Ultramicroscopy* **63**, 169–179 (1996).
52. J. Vörös, The density and refractive index of adsorbing protein layers. *Biophys. J.* **87**, 553–561 (2004).
53. R. Yan *et al.*, Simultaneous determination of sample thickness, tilt, and electron mean free path using tomographic tilt images based on Beer-Lambert law. *J. Struct. Biol.* **192**, 287–296 (2015).
54. J. Hattne, "Low-dose data collection and radiation damage in MicroED" in *CryoEM*, T. Gonen, B. L. Nannenga, Eds. (*Methods in Molecular Biology*, Springer US, 2021), pp. 309–319.
55. M. J. Berger, J. S. Coursey, M. A. Zucker, J. Chang, "Stopping-power and range tables for electrons, protons, and helium ions" (NIST Physics Laboratory Gaithersburg, MD, 1998).
56. C. Nave, M. A. Hill, Will reduced radiation damage occur with very small crystals? *J. Synchrotron Radiat.* **12**, 299–303 (2005).
57. J. Schindelin *et al.*, Fiji: An open-source platform for biological-image analysis. *Nat. Methods* **9**, 676–682 (2012).